Continuous Soluble Ziegler-Natta Ethylene Polymerizations in Reactor Trains. I. Mathematical Modeling

MARCELO EMBIRUÇU,[1,2] ENRIQUE LUIS LIMA,[1] JOSÉ CARLOS PINTO[1]

[1] Programa de Engenharia Química/COPPE, Universidade Federal do Rio de Janeiro, Cidade Universitária, CP:68502, Rio de Janeiro 21945-970 RJ, Brazil

[2] Departamento de Engenharia Química, Universidade Federal da Bahia, Rua Aristides Novis, 2 Federação, Salvador 40210-630 BA, Brazil

Received 16 August 1999; accepted 21 January 2000

ABSTRACT: A detailed mathematical model is developed to describe the dynamics of continuous soluble Ziegler-Natta ethylene polymerizations in reactor trains composed of series of both stirred tank and tubular reactors. The model comprises a detailed description of the reaction mechanism and the mass, energy, and momentum balance equations for each reactor vessel, which are then used to allow the prediction of final polymer properties (average polymer molecular weights, polymer density, melt flow index, etc.) and process performance (polymer productivity, head losses, energy consumption, etc.). Tubular reactors are assumed to behave as ideal plug flow reactors, and the method of characteristics is used to solve the set of algebraic-partial differential equations that describe the process. Plant data are used to validate the model, which is shown to describe very well the operation of actual industrial reactors. © 2000 John Wiley & Sons, Inc. J Appl Polym Sci 77: 1574–1590, 2000

Key words: soluble; Ziegler-Natta; ethylene; polymerization; reactor; mathematical model

INTRODUCTION

Mathematical models are of paramount importance for polymerization engineering, as final polymer properties, and process responses depend upon the process operation conditions in a very complex and nonlinear manner.[1,2] This is particularly true for soluble ethylene Ziegler-Natta polymerizations, as the reaction mechanism comprises a large number of reaction steps and the kinetic behavior of the catalyst species depends on many operation variables.[2,3]

Polyethylene (PE) is the most produced thermoplastic in the world, which shows that proper understanding of PE manufacture is of great economical importance. PE is produced nowadays through four different basic technological routes: suspension (slurry) polymerizations, solution polymerizations, gas-phase polymerizations, and bulk high-pressure polymerizations. In spite of the continuous shift toward the development of continuous gas-phase polymerizations, the other technological routes are still of great economical importance, because some polymer grades cannot be produced in gas phase.

Solution processes present some advantages when compared to suspension processes. First, molecular weight distributions (MWDs) of final polymer and other process variables are controlled more easily because of the homogeneous nature of the reaction environment. Besides, po-

Correspondence to: J. C. Pinto (pinto@peq.coppe.ufrj.br).
Contract grant sponsor: Conselho Nacional de Desenvolvimento Científico e Tecnológico.
Contract grant sponsor: Politeno Ind. e Com. S. A.
Contract grant sponsor: PADCT.
Contract grant sponsor: PRONEX.

Journal of Applied Polymer Science, Vol. 77, 1574–1590 (2000)

lymerization may occur at higher temperatures, which leads to larger reaction rates and polymer productivities. However, high and ultra-high molecular weights cannot be attained at solution processes because of the higher temperatures, and the morphology of the final polymer powder cannot be controlled as tightly as in heterogeneous media. Because of the smaller residence times needed to produce solutions of high polymer concentrations, smaller reactors may be used in solution processes, which allows faster transitions between different grades and low production rates of off-spec material. When compared to gas-phase processes, solution reactors permit a better control of polymerization temperature, but require the installation of solvent recovery facilities. Finally, molecular architecture of the final polymer material produced in solution is much more regular than the molecular architecture of the polymer material produced at high-pressure reactors, which is well known for its high branching frequency and low density.

Despite the large number of articles published regarding the kinetics of heterogeneous Ziegler-Natta catalysts and the operation of heterogeneous olefin polymerization reactors and the relatively large number of industrial sites (about 10–20) that use the solution technology for ethylene polymerization, the literature related to solution Ziegler-Natta polymerizations is relatively scarce. Choi[4] studied the solution ethylene polymerization in continuous stirred tank reactors using Ziegler-Natta catalysts and developed a kinetic model that allowed fair description of the reactor operation and the development of control policies for proper control of the MWD of the final polymer. Cozewith[5] studied the ethylene/propylene/ethylidene terpolymerization in solution and developed a mathematical model based on a very detailed kinetic mechanism for industrial Ziegler-Natta continuous stirred tank reactors, which allowed good description of transient responses of actual polymerization reactions. Kim and Choi[6] studied the Ziegler-Natta solution ethylene/1-butene copolymerization in continuous stirred tank reactors and developed a kinetic model that allowed good prediction of available industrial data.

The interesting point regarding the solution technology is that industrial facilities generally comprise different reactor vessels that may be operated independently or in series. Therefore, the process operation is usually very flexible and allows the production of different polymer grades with short transient times, given the usually small residence times used. However, it seems that these interesting process characteristics have been completely overlooked in the public literature. Useful mathematical models for solution processes must include a detailed kinetic model to describe the complex chemistry of soluble Ziegler-Natta polymerizations and software modules for simulation of process operation in reactor series containing arbitrary number of continuous stirred tank and tubular reactors. The model also should allow the simulation of complex flowsheets, containing an arbitrary number of interconnections among the reactor vessels in the process.

The main objective of this article is to develop mathematical models for Ziegler-Natta solution ethylene polymerizations in continuous stirred tank and tubular reactors in order to allow the simulation of actual industrial plant sites that comprise trains of reaction vessels interconnected arbitrarily. Models must allow the prediction of both final polymer properties (average polymer molecular weights, polymer density, melt flow index) and process performance (polymer productivity, head losses, energy consumption). Models are validated through simulations carried out at conditions that resemble actual industrial operation conditions. It will be shown below that the mathematical model is able to reproduce extremely well the steady-state and transient responses of industrial plants in two typical process configurations.

Process Description

The process studied is the solution ethylene polymerization using soluble Ziegler-Natta catalysts in trains of continuous stirred tank and tubular reactors. The feed stream is assumed to be a mixture of ethylene, 1-butene, solvent (cyclohexane), a mixture of Ziegler-Natta catalysts and cocatalysts, and hydrogen. Catalysts and cocatalysts are precontacted before being fed to the reactor vessels, so that it may be assumed that catalysts are fed in their active form. Feed streams with different compositions may be inserted into different process locations, so that feed policies are very flexible. The most important points regarding the catalyst systems used and the process configuration are discussed below.

The Catalyst Systems

Different Ziegler-Natta catalysts are used at plant site, but numerical examples in this paper

will regard a specific catalyst system. As shown by Embiruçu et al.,[7] the model is able to describe effectively the process behavior when different catalyst systems are analyzed. Although a detailed description of the catalyst systems cannot be provided for proprietary reasons, it is important to say that the catalyst feed is a mixture containing varying amounts of $TiCl_4$ and $VOCl_3$ as active catalyst species, which must be activated by TEA (triethyl aluminum) prior to polymerization. The catalyst used here is called as the standard catalyst or catalyst A. The catalyst activation operation is carried out at the catalyst feed tanks, so that catalyst species are fed in the activated form. The activation temperature may be used as a control variable for process operation, but will be neglected in this study because the activation mechanism is not very well understood and because the activation temperature is manipulated to produce small amounts of very specific polymer grades. As the catalyst is still very active at the outlet stream, chemicals are added to the output stream to promote catalyst deactivation and avoid polymer degradation and oligomer production.

Process Configuration

The process studied here is composed of two tubular reactors (reactors 1 and 3) and a non-ideal stirred tank reactor (reactor 2). The operation is adiabatic and cooling devices are not used. The basic process configuration is shown in Figure 1. As shown in Figure 1, different operation modes may be used in this system, as all reactor vessels are equipped with injection points for all chemical species. Usually, monomer, comonomer, solvent, hydrogen, catalysts, and cocatalysts are fed into the first reactor of the series (which may be reactor 1 or reactor 2), and hydrogen is injected along the reactor train to modify the resin grade. Reactor 3 is used as a trimmer, to increase monomer conversion and reduce the amounts of residual light gases at the output stream. Besides, the agitators of reactor 2 may be turned off in order to allow the operation of this vessel as a tubular reactor of large diameter. Therefore, depending on the operation mode, the process may be composed of a series of tubular reactors, a continuous stirred tank reactor or some other type of mixed configuration. By changing the operation mode, significant changes of the MWD of the final polymer may be obtained, allowing the production of many resin grades.

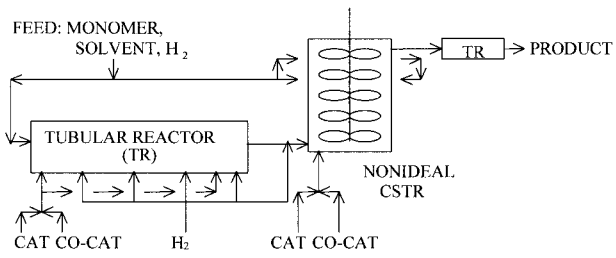

Figure 1 Basic process configuration.

Two operation modes are used most often:

Configuration 1: agitated mode. Reactor 1 is not used and the agitators of reactor 2 are turned on. Two monomer feed points and one catalyst feed point are used. Lateral feed points are used to improve the degree of mixing inside the stirred tank reactor. The degree of mixing is controlled through the manipulation of the agitator speed and the lateral feed flow rate. Backmixing inside the stirred tank reactor is forced by the agitator work, but relatively distinct mixing zones are present and axial temperature gradients may be observed. The process is composed of a nonideal stirred tank and a tubular reactor in series and is used to produce polymer grades with narrower MWDs.

Configuration 2: tubular mode. Monomer and catalysts are injected into reactor 1 and hydrogen is injected along the reactor train to control the MWD. The agitators of reactor 2 are turned off, so that the process is composed of three tubular reactor in series. The proper control of the feed temperature is of fundamental importance in this mode, to avoid polymer precipitation inside the reactor. This operation mode is used to produce polymer grades with broader MWDs.

Despite the very small residence times in reactor 2 and the fact that agitators are turned off when plant operation is performed in the tubular mode, a significant amount of mixing always occurs in this reaction vessel, because its large diameter and internals (agitators, baffles) act as static mixers and favor dispersion. Extensive simulation studies[8] showed that reactor 2 behaves as a series of non ideal CSTRs even in the tubular mode. Attempts to model this piece of equipment as a standard plug flow or a standard dispersion reactor in configuration 2 were unsuccessful because this would require the estimation of different sets of kinetic constants for the two different operation modes, which is not acceptable. On the contrary, the assumption that the reactor behaves as a nonideal CSTR train allowed the estimation of a single set of kinetic constants for both

Table I Kinetic Mechanism

Reaction Steps		Rate Equation
Instantaneous steps		
Active site formation	$C + CC \rightarrow C^*$	Infinite
Catalyst poisoning	$I_{CC} + CC \rightarrow CCD$	Infinite
	$I_{C^*} + C^* \rightarrow CD$	Infinite
Chain initiation	$C^* + M \underset{k_p}{\overset{k_i}{\rightarrow}} P_1$	$k_i \cdot [C^*] \cdot [M]$
Chain propagation	$P_j + M \longrightarrow P_{j+1}$	$k_p \cdot [P_j] \cdot [M]$
Chain transfer		
To hydrogen	$P_j + H_2 \underset{k_{fM}}{\overset{k_{fH}}{\longrightarrow}} C^* + U_j$	$k_{fH} \cdot [P_j] \cdot [H_2]^{1/2}$
To monomer	$P_j \underset{k_f}{+} M \longrightarrow P_1 + U_j$	$k_{fM} \cdot [P_j] \cdot [M]$
Espontaneous	$P_j \rightarrow C^* + U_j$	$k_f \cdot [P_j]$
To alkyl aluminum	$P_j + CC \underset{k_{fCC}}{\longrightarrow} C^* + U$	$k_{fCC} \cdot [P_j] \cdot [CC]^{1/2}$
Termination		
Espontaneous deactivation	$C^* \overset{k_d}{\longrightarrow} CD$	$k_d \cdot [C^*]$
Termination with hydrogen	$P_j + H_2 \underset{k_{tM}}{\overset{k_{tH}}{\longrightarrow}} CD + U_j$	$k_{tH} \cdot [P_j] \cdot [H_2]^{1/2}$
Termination with monomer	$P_j \underset{k_t}{+} M \longrightarrow CD + U_j$	$k_{tM} \cdot [P_j] \cdot [M]$
Espontaneous termination	$P_j \rightarrow CD + U_j$	$k_t \cdot [P_j]$

C^* is the active species, CC is the cocatalyst, I_{C^*} are catalyst poisons, I_{CC} are cocatalyst poisons, CCD is the inactive cocatalyst, CD is the inactive catalyst, H_2 is hydrogen, M is monomer, P_j is a live polymer chain with size j and U_j is a dead polymer chain with size j.

operation modes when the same catalyst is used, as shown below.

Kinetic Model

Very little is known about the kinetics of soluble Ziegler-Natta polymerizations, despite some very detailed mechanistic studies available in the literature.[9–12] This is because detailed analysis of rate data and MWDs have not been published in the open literature. A detailed kinetic model may be developed if an intensive study involving experimental design, rate, and MWD data analysis and use of parameter estimation procedures is carried out, which is beyond the scope of this work. The kinetic model developed and used here is based on published data and process data obtained at the plant site. For this reason, the kinetic mechanism is kept as simple as possible in order to describe the most important characteristics of the process operation and catalyst properties and to reduce the number of kinetic parameters to be estimated.

The kinetic mechanism used here may be regarded as a modification of the mechanisms presented by Cozewith[5] and Kim and Choi,[6] which were used as a basis for this work. A modification was the inclusion of chain termination and catalyst deactivation promoted by hydrogen, as observed for certain catalyst systems and supported by kinetic studies of Matsuda and Keii for ethylene polymerizations with different Ziegler-Natta catalysts.[9] Chain initiation and catalyst inhibition by impurities also had to be included in the kinetic model, in order to allow the proper interpretation of plant data, as unknown impurities are generally present in the monomer and solvent feed streams. The detailed kinetic mechanism for homopolymerization is presented in Table I.

The mechanism may be extended for copolymerization reactions in a straightforward manner, by including the reaction steps that involve the second monomer and including cross-reaction steps, if the ultimate kinetic mechanism is assumed. This will not be done here because of the lack of experimental data needed to evaluate the kinetic parameters. Besides, because the comonomer is added in small amounts (when it is added to the feed stream) and is about 30 times less reactive than ethylene (so that comonomer conversion is always low), the effect of comonomer on the final polymer properties is modeled empiri-

cally, as discussed afterwards. Therefore, the homopolymerization kinetic scheme is also used to describe the kinetics of copolymerization.

Regarding the catalyst sites, it is important to emphasize that multiple catalyst sites with different activities are present in the reaction environment. Therefore, sets of kinetic constants are needed for each individual catalyst site. The presence of multiple active sites is due to the use of mixtures of transition metal based compounds to sinthesize the catalyst species, is due to incomplete reduction of the transition metal atoms during the catalyst preparation,[9] and is also due to incomplete complexation and over-complexation of the transition metal during catalyst activation.[12] For this reason, it is known that the use of cocatalyst in excess may cause catalyst deactivation.[13] However, because catalyst/cocatalyst ratios used during catalyst preparation and activation are not allowed to vary very much at plant site and because state variables, such as reactor temperatures and concentrations, are subject to large variations along the reactor train, very little is gained by increasing the number of catalyst sites in the kinetic model. Therefore, unless stated otherwise, the number of active species is always assumed to be equal to one, which means that a smaller number of kinetic constants should be estimated and that the kinetic constants actually describe the average behavior of the catalyst mixture. This assumption would have to be relaxed if one was interested in describing the detailed shape of the MWD of the final polymer, which is not done here.

Table I shows that impurities (poisons) are assumed to reduce the number of catalyst and cocatalyst molecules in the reaction environment. This is a very simple description of the kinetics of inhibition and poisoning. However, from a realistic point of view, the kinetics of inhibition cannot be modeled otherwise, because impurities are generally unknown and are present in the reaction environment at unknown concentrations. Several impurities may affect the solution Ziegler-Natta ethylene polymerizations, such as water, ketones, organic acids, alcohols, carbon monoxide, carbon dioxide, oxygen, sulfur compounds, etc. Some of these impurities also can affect the MWD of the final polymer, by acting as chain transfer agents. This effect is neglected in this work.

Table I shows that several chain transfer reactions are assumed to be possible. However, at the plant site hydrogen is certainly the most important chain transfer agent and is used to design the MWD of the final polymer. As shown by Marques et al.[14,15] and van der Ven,[13] it is believed that the hydrogen molecule has to adsorb and dissociate over the catalyst surface before chain transfer reaction can take place, which justifies the hydrogen order 0.5 used to describe the reaction rate.

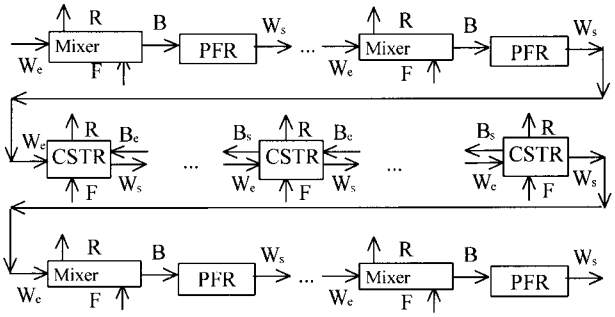

Figure 2 Physical modeling of the process flowsheet.

Another important point regards the catalyst stability. The catalyst activity decays very fast in theses systems and the half-life time of the catalyst species is of the order of seconds to a few minutes.[13] Table I presents a compilation of termination effects reported in the literature and at plant site.[13]

Mathematical Model

The mathematical model developed is based on the physical representation of the process flowsheet shown in Figure 2. The representation is very flexible and allows the simulation of all operation modes of the process described before. The existence of multiple feed points is modeled through a series of reactors separated by ideal mixers. The nonideal stirred tank reactor is modeled as a series of ideal CSTRs with reflux streams that provide reactor backmixing. Alternative flowsheets also may be simulated, because computer codes were programmed modularly.

In order to write the balance equations, the well-known method of moments (see Ray[16]) is used to describe the first statistical averages of the MWD of both live and dead polymer chains.

Balance Equations for CSTRs

The global mass balance for CSTR r may be given by

$$\frac{dM_r}{dt} = W_{(r-1)} + F_r + B_{(r+1)} - R_r - B_r - W_r + G_r \tag{1}$$

Assuming that the reactor volume is constant, eq. (1) may be written as

$$W_r = W_{(r-1)} + F_r + B_{(r+1)} - R_r - B_r - V_r \cdot \frac{d\rho_r}{dt}$$

$$r = 1 \Rightarrow B_r = 0 \quad r = Nr \Rightarrow B_{(r+1)} = 0 \tag{2}$$

where ρ is the density of the reacting mixture. The backmixing stream B is assumed to be a function of the agitator speed, of the lateral feed flow rates, and of the reactor geometry. Besides, it is assumed that these functions are additive and decrease as solution viscosity increases. Based on these assumptions, the following empirical model is proposed:

$$B_r = \frac{\rho_r \cdot V_r}{\mu_r} \cdot (D_0 + D_1 \cdot I + D_f \cdot f)$$

$$r = 1 \Rightarrow B_r = 0 \quad r = Nr \Rightarrow B_{(r+1)} = 0 \tag{3}$$

where μ is the viscosity of the polymer solution, I is the electrical current consumed by the agitator (an indirect measurement of the agitator speed), f is the lateral feed flow rate of reactor r (as a fraction of the total feed flow rate), and D_0, D_{Rotr}, and D_f are coefficients to be estimated. Equation (3) is based on actual data available at plant site and could be improved if detailed modeling of the flow is needed. However, as process values are constrained within relatively narrow intervals, more detailed modeling of backmixing was not necessary.

Based on a constant reactor volume, the individual mass balance equations may be written as

$$\frac{d[C]_r}{dt} = \frac{W_{(r-1)} \cdot [C]_{(r-1)}}{\rho_{(r-1)} \cdot V_r} + \frac{F_r \cdot [C]_{F_r}}{\rho_{F_r} \cdot V_r} + \frac{B_{(r+1)} \cdot [C]_{(r+1)}}{\rho_{(r+1)} \cdot V_r} - \frac{(R_r + B_r + W_r) \cdot [C]_r}{\rho_r \cdot V_r} + r_{C_r}$$

$$r = 1 \Rightarrow B_r = 0 \quad r = Nr \Rightarrow B_{(r+1)} = 0$$

$$C = \lambda_0,\ \lambda_1,\ \lambda_2,\ EA_n = (C_n^* + \mu_{0,n}),\ CD_n,\ M,\ H_2,\ CC,\ S \tag{4}$$

where individual reaction rates are presented in Table I. For the other chemical species present in the reacting system, the quasi steady-state assumption was used and led to the equations presented below.

Assuming that kinetic and potential energy terms and that the work made by the agitator can be neglected, that operation is adiabatic, under rather standard kinetic assumptions the energy balance may be presented as

$$\frac{dT_r}{dt} = \frac{\sum_{e=F_r,W_{r-1},B_{r+1}}^{NKE} W_e \cdot \left[\int_r^e Cp_u \cdot dT + \frac{[M]_e \cdot PM_m}{\rho_e} \cdot \left(\int_r^e Cp_m \cdot dT - \int_r^e Cp_u \cdot dT \right) + \frac{[S]_e \cdot PM_s}{\rho_e} \cdot \left(\int_r^e Cp_s \cdot dT - \int_r^e Cp_u \cdot dT \right) \right] + V_r \cdot r_{E,r}}{\rho_r \cdot V_r \cdot Cp}$$

$$r = 1 \Rightarrow B_r = 0 \quad r = Nr \Rightarrow B_{(r+1)} = 0 \tag{5}$$

where

$$r_{E,r} = r_{p,r} \cdot \left(\Delta HN_p^0 + PM_m \cdot \int_0^r (Cp_u - Cp_m) \cdot dT \right) \tag{6}$$

which takes into account the fact that reaction conditions can vary significantly along the reactor train, so that physical properties cannot be regarded as constants.

Balance Equations for Tubular Reactors

As described previously, because of the very short residence times, tubular reactors were modeled using standard plug flow assumptions. Therefore, the global mass balance may be written as

$$\frac{\partial \rho}{\partial t} = -\frac{\partial(\rho \cdot v)}{\partial z} \Leftrightarrow \frac{\partial \rho}{\partial t} = -\frac{\partial\left(\rho \cdot \frac{W}{\rho \cdot A}\right)}{\partial z} \Rightarrow$$

$$\frac{\partial \rho}{\partial t} = -\frac{1}{A} \cdot \frac{\partial(W)}{\partial z} \tag{7}$$

where W is the mass flow rate, v is the flow velocity, z is the axial position, and A is the transversal flow area.

Individual mass balance equations may be written as

$$\frac{\partial(v \cdot [C])}{\partial z} + \frac{\partial [C]}{\partial t} = r_c \tag{8}$$

where C assumes the same values presented in Eq. (4).

Based on the same assumptions presented before, the energy balance may be written as

$$\frac{\partial T}{\partial t} = -\frac{W}{\rho \cdot A} \cdot \frac{\partial T}{\partial z} + \frac{r_E}{\rho \cdot C_p} \Leftrightarrow \frac{\partial T}{\partial t} + v \cdot \frac{\partial T}{\partial z} = \frac{r_E}{\rho \cdot Cp} \tag{9}$$

Balance Equations for Ideal Mixers

The assumptions made are very similar to the ones made before. Additionally, it is assumed that the mixer dynamics may be neglected. Therefore, the global mass balance equation may be written as

$$W_s = W_e + W_f - W_a \tag{10}$$

The individual mass balance equations may be written as

$$[C]_s = \frac{\dfrac{[C]_e \cdot W_e}{\rho_e} + \dfrac{[C]_f \cdot W_f}{\rho_f}}{WQ_s} \tag{11}$$

$$C = \lambda_0,\ \lambda_1,\ \lambda_2,\ EA_n = (C_n^* + \mu_{0,n}),\ CD_n,\ M,\ H_2,\ CC,\ S$$

where

$$WQ_s = \frac{W_{m,e} + W_{m,f}}{\rho_{m,s}} + \frac{W_{s,e} + W_{s,f}}{\rho_{s,s}} + \frac{W_{u,e} + W_{u,f}}{\rho_{u,s}} \tag{12}$$

and

$$W_{i,k} = \frac{PM_i \cdot [I]_k \cdot W_k}{\rho_k} \quad k = e,\ f,\ s \tag{13}$$

$$W_{u,k} = \frac{PM_m \cdot \lambda_{l,k} \cdot W_k}{\rho_k} \tag{14}$$

Finally, the energy balance may be presented as

$$W_e \cdot \left(\int_s^e Cp_u \cdot dT + \frac{[M]_e \cdot PM_m}{\rho_e} \cdot \left(\int_s^e Cp_m \cdot dT - \int_s^e Cp_u \cdot dT \right) + \frac{[S]_e \cdot PM_s}{\rho_e} \cdot \left(\int_s^e Cp_s \cdot dT - \int_s^e Cp_u \cdot dT \right) \right) + W_f \cdot \left(\int_s^f Cp_u \cdot dT + \frac{[M]_f \cdot PM_m}{\rho_f} \cdot \left(\int_s^f Cp_m \cdot dT - \int_s^f Cp_u \cdot dT \right) + \frac{[S]_f \cdot PM_s}{\rho_f} \cdot \left(\int_s^f Cp_s \cdot dT - \int_s^f Cp_u \cdot dT \right) \right) = 0 \tag{15}$$

Individual reaction Rates

Based on Table I, the following rate equations may be written for each individual chemical species analyzed:

$$r_{EA_n} = -\mu_{0,n} \cdot (k_{fH,n} \cdot [H_2]^{ofH} + k_{f,n} + k_{fCC,n} \cdot [CC]^{ofCC}) - k_{d,n} \cdot [C_n^*] \tag{16}$$

$$r_{CD_n} = \mu_{0,n} \cdot (k_{tH,n} \cdot [H_2]^{otH} + k_{tE,n} \cdot [M] + k_{t,n}) + k_{d,n} \cdot [C_n^*] \Leftrightarrow r_{CD_n} = -r_{EA_n} \tag{17}$$

$$r_M = [M] \cdot \sum_{n=1}^{NSIT} \left\{ \begin{matrix} -k_{i,n} \cdot [C_n^*] - k_{p,n} \cdot \mu_{0,n} - k_{fE,n} \cdot (\mu_{0,n} - [P_{l,n}]) \\ -k_{tE,n} \cdot (\mu_{0,n} - [P_{l,n}]) \end{matrix} \right\} \tag{18}$$

$$r_{H_2} = [H_2]^{ofH} \cdot \sum_{n=1}^{NSIT} \mu_{0,n} \cdot (-k_{fH,n}) + [H_2]^{otH} \cdot \sum_{n=1}^{NSIT} \mu_{0,n} \cdot (-k_{tH,n}) \tag{19}$$

$$r_{CC} = -[CC]^{ofCC} \cdot \sum_{n=1}^{NSIT} k_{fCC,n} \cdot \mu_{0,n} \quad (20)$$

$$r_{\lambda,n} = (k_{fH,n} \cdot [H_2]^{ofH} + k_{tH,n} \cdot [H_2]^{otH}) + [M] \cdot (k_{fE,n} + k_{tE,n}) + k_{fCC,n} \cdot [CC]^{ofCC} + k_{f,n} + k_{t,n} \quad (21)$$

$$r_{\lambda_m} = \sum_{n=1}^{NSIT} \mu_{m,n} \cdot r_{\lambda,n}$$

$$r_S = 0 \quad (22)$$

where

$$k_j = A_j \cdot \exp\left(\frac{-E_j}{R \cdot T}\right)$$

$$j = d, i, p, fH, fE, f, fCC, tH, tE, t \quad (23)$$

Moments of Live Polymer Chains

Although Cozewith[5] considers that the lifetime of growing polymer chains is too high for quasi steady-state assumptions to be valid, Kim and Choi[6] showed through simulation that this would be a good hypothesis for the system analyzed. Assuming that the quasi steady-state assumption is valid for growing polymer chains, the following equations may be written:

$$\mu_{0,n} = \frac{r_{i,n}}{f_{cP,n} - f_{p,n} - f_{fE,n}} \quad (24)$$

$$\mu_{1,n} = \frac{[P_{l,n}]}{\left(1 - \frac{f_{p,n}}{f_{cP,n}}\right)^2} \quad (25)$$

$$\mu_{2,n} = \frac{\left(1 + \frac{f_{p,n}}{f_{cP,n}}\right) \cdot [P_{l,n}]}{\left(1 - \frac{f_{p,n}}{f_{cP,n}}\right)^3} \quad (26)$$

where

$$f_{cP,n} = [M] \cdot (k_{p,n} + k_{fE,n} + k_{tE,n}) + (k_{fH,n} \cdot [H_2]^{ofH} + k_{tH,n} \cdot [H_2]^{otH}) + k_{fCC,n} \cdot [CC]^{ofCC} + k_{f,n} + k_{t,n} \quad (27)$$

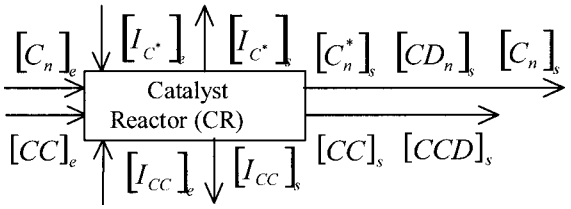

Figure 3 The catalyst reactor.

$$f_{p,n} = k_{p,n} \cdot [M] \quad (28)$$

$$f_{fE,n} = k_{fE,n} \cdot [M] \quad (29)$$

$$r_{i,n} = k_{i,n} \cdot [C_n^*] \cdot [M] \quad (30)$$

Therefore, the total active catalyst concentration may be given by

$$[C_n^*] = [EA]_n - \mu_{0,n} \quad (31)$$

Catalyst Activation and Poisoning

The operation of catalyst activation and the influence of impurities on the reactor operation is modeled as shown in Figure 3, based on the discussion already presented. It is assumed that before being added to the system, the feed stream is filtered by a "Catalyst Reactor," where catalyst activation and poisoning occur instantaneously.

Because reaction rates are very fast, the balance equations always provide trivial solutions, in the sense that reactants that are not added in excess are completely consumed by the activation/poisoning steps, whereas the other chemical species are partially consumed. For the most important case, for instance, when catalyst and cocatalyst are added in excess in relation to impurities and cocatalyst is added in excess in relation to catalyst, the following solution may be obtained:

$$[I_{CC}] = 0 \quad (32)$$

$$[I_{C^*}] = 0 \quad (33)$$

$$[CC] = [CCD]_e - [I_{CC}]_e - \sum_{n=1}^{NCAT} [C_n]_e \quad (34)$$

$$[CCD] = [CCD]_e + [I_{CC}]_e \quad (35)$$

$$[C_n] = 0 \quad (36)$$

$$[C_n^*] = \frac{\left(\sum_{n=1}^{NCAT} [C_n^*]_e + \sum_{n=1}^{NCAT} [C_n]_e - [I_{C^*}]_e \right) \cdot ([C_n^*]_e + [C_n]_e)}{\sum_{n=1}^{NCAT} [C_n^*]_e + \sum_{n=1}^{NCAT} [C_n]_e} \quad (37)$$

$$[CD_n] = [CD_n]_e + [C_n]_e + [C_n^*]_e - [C_n^*] \quad (38)$$

The solution may be presented in a much more general way, as shown by Embiruçu,[8] taking into account all other possibilities. However, eqs. (32)–(38) are good enough for the purposes of this work.

Momentum Balance

Pressure decreases steadily along the reactor train and is an important variable for process monitoring. A rigorous momentum balance may be performed in order to describe head losses through the reactor train, but this leads to significant increase of the numerical complexity of the model and usually cannot be justified, because much simpler approaches may provide an excellent description of head losses in the system. It is assumed here that an empirical equation may be used to describe head losses in the form

$$\Delta P = K \cdot \mu \cdot WQ^2 \quad (39)$$

where K is a coefficient to be determined and μ is the viscosity of the polymer solution, and WQ is the volumetric flow rate of the polymer solution. Because monomer conversions are always close to 100% and polymer concentrations vary within a relatively narrow interval, Eq. (39) may be written in a much more convenient way:

$$\Delta P = K \cdot \mu \cdot W_u^2 \quad (40)$$

where W_u is the rate of polymer production.

Physical Properties

Assuming that volume additivity holds for densities and that mass additivity holds for heat capacities, the following equations may be written:

$$\rho_r = \frac{[M]_r \cdot PM_m}{\rho_{m,r}} \cdot (\rho_{m,r} - \rho_{u,r}) + \frac{[S]_r \cdot PM_s}{\rho_{s,r}} \cdot (\rho_{s,r} - \rho_{u,r}) + \rho_{u,r} \quad (41)$$

$$\frac{d\rho_r}{dt} = PM_m \cdot \frac{(\rho_{m,r} - \rho_{u,r})}{\rho_{mr}} \cdot \frac{d[M]_r}{dt} + PM_s \cdot \frac{(\rho_{s,r} - \rho_{u,r})}{\rho_{sr}} \cdot \frac{d[S]_r}{dt} + \left\{ [M]_r \cdot PM_m \cdot \left(\frac{\rho_{u,r} \cdot \frac{df_m(T_r)}{dT_r} - \rho_{m,r} \cdot \frac{df_u(T_r)}{dT_r}}{\rho_{m,r}^2} \right) + [S]_r \cdot PM_s \cdot \left(\frac{\rho_{u,r} \cdot \frac{df_s(T_r)}{dT_r} - \rho_{s,r} \cdot \frac{df_u(T_r)}{dT_r}}{\rho_{s,r}^2} \right) + \frac{df_u(T_r)}{dT_r} \right\} \cdot \frac{dT_r}{dt} \quad (42)$$

$$Cp = Cp_{u,r} + \frac{[M] \cdot {}_rPM_m}{\rho_r} \cdot (Cp_{m,r} - Cp_{u,r}) + \frac{[S] \cdot {}_rPM_s}{\rho_r} \cdot (Cp_{s,r} - Cp_{u,r}) \quad (43)$$

where

$$\rho_{i,r} = f_i(T_r) \quad (44)$$

are known functions of temperature for each individual component. As said before, Cp is also a known function of temperature for each chemical species.

As the viscosity of the polymer solution depends basically on the MWD of the polymer produced, as polymer concentrations do not vary very much, it may be related to the melt flow index of the polymer as[17]:

$$\mu = a \cdot MI^b \quad (45)$$

where a and b are coefficients to be determined.

Output Variables and End-Use Properties of Polymer

Based on the model state variables, some useful variables may be defined. For instance, monomer conversion may be defined as

$$x_z = 100 \cdot \frac{\lambda_{1,z}}{[M]_z + \lambda_{1,z}} \tag{46}$$

where x is conversion and z indicates the axial position.

Average molecular weights may be computed as

$$\overline{PM}_m = PM_m \cdot \frac{\mu_2 + \lambda_2}{\mu_1 + \lambda_1}$$

$$\overline{PM}_n = PM_m \cdot \frac{\mu_1 + \lambda_1}{\mu_0 + \lambda_0}$$

$$PD = \frac{\overline{PM}_m}{\overline{PM}_n} \tag{47}$$

where $\overline{PM}_m$ is the weight average molecular weight, $\overline{PM}_n$ is the number average molecular weight, and PD is the polydispersion index.

A value that is commonly used at plant site to characterize the final polymer resin is the melt flow index (MI). The MI may be defined as the mass of polymer that flows in 10 min through an orifice at a defined temperature when subject to a specified pressure. The MI is essentially an indirect measurement of viscosity and weight average molecular weight. The larger the MI, the lower the weight average molecular weight. Because MI measurements are much cheaper and faster than other techniques used to evaluate average molecular weights, MI evaluations are very popular at plant sites. Although it is known that the correlation between the MWD and the flow behavior of polymer melts may be rather complex (see Carrot et al.[18]), a typical empirical model used at plant site for MI has the following form (Gahleitner et al.[19,20]):

$$MI = \alpha \cdot Mw^{\beta} \tag{48}$$

Figure 4 shows results obtained when eq. (48) is used to describe how the MI of solution polyethylenes depend on weight average and number average molecular weights. Experimental data were obtained at plant site.[21] Figure 4 shows that there is an excellent correlation between the MI and the weight average molecular weight of the final polymer. It must be pointed out that it is not necessary to modify eq. (48) to take into consideration the amount of 1-butene incorporated into the final polymer resin. This is additional evidence of the low degree of incorporation of comonomer and also an indication that 1-butene is not an important chain transfer agent for the reaction system studied. As said before, hydrogen is the most important control variable for MI and the final MWD of the polymer.

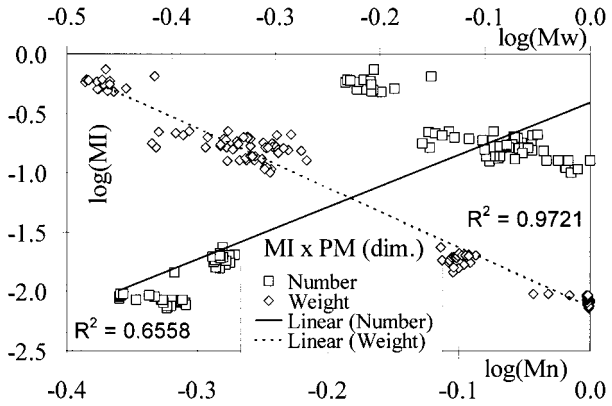

Figure 4 Power law correlations between MI and number average and weight average molecular weights of final polymer.

Another value that is commonly used to characterize the final polymer resin at plant site is the stress exponent (SE), defined as

$$SE = \frac{\log(MI[3 \cdot p]/MI)}{\log(3)} \tag{49}$$

where p represents the load used to evaluate the MI. Therefore, the SE is a type of ratio between values of MI obtained when different loads are used to force the melt flow through the standard orifice. As defined by eq. (49), SE is a measure of the non-Newtonian character of the polymer melt and may be used to evaluate the processability of the polymer resin. Embiruçu[8] shows that the SE may be closely related to PD, which means that an empirical model may be used to describe how the SE depends on the broadness of the MWD of final polymer. By mixing empirical and theoretical reasoning, Embiruçu[8] shows that the following function may be used to correlate SE and PD:

$$SE = \frac{1}{\frac{1}{SE_M} + \frac{\left(\frac{1}{SE_m} - \frac{1}{SE_M}\right)}{\exp(\beta)} \cdot \exp(\beta \cdot PD)} \tag{50}$$

Figure 5 illustrates how eq. (50) may be used to evaluate the polymer polydispersion.

Another important property of the final polymer is the bulk density of the polymer powder. This property is typically used as a measure of

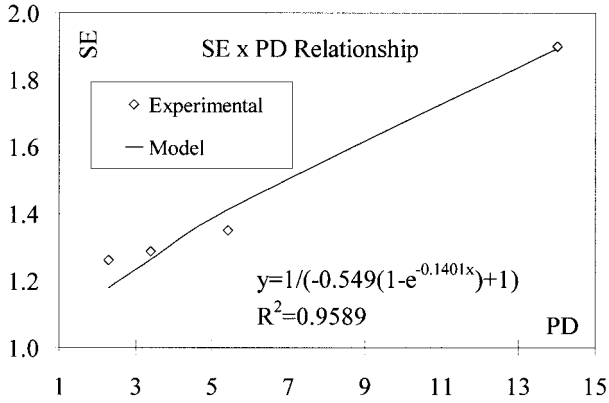

Figure 5 Correlation between SE and polydispersity.

polymer crystallinity and degree of branching of polymer chains. In copolymer grades, it may be related to the final copolymer composition, as comonomer molecules introduce short branches into the polymer chain and cause a reduction of polymer crystallinity and bulk density. As polymer crystallinity also depends on the average molecular weights and polydispersion, it may be concluded that density is not an unequivocal measurement of polymer composition, but depends on the availability of MI and SE measurements.

Figure 6 shows results obtained when the homopolymer density is assumed to be a function of SE, MI, and comonomer feed concentration, as suggested by Schultz.[21] It is important to emphasize that the independent variables selected describe the MWD and composition of the final polymer resin in an indirect manner.

$$\rho = \alpha + \beta \cdot \log(MI) + \gamma \cdot SE + \delta \cdot [CM]_e^{\varepsilon} \quad (51)$$

It may be seen that there is a fair correlation between the variables analyzed.

Numerical Procedure

The mathematical model comprises a relatively large set of partial-differential algebraic equations, which must be solved simultaneously. In order to explain the numerical procedure, though, it is interesting to separate the model equations into modules, which are provided by the tubular reactors, stirred tank reactors, and mixers.

The partial-differential equations that constitute the tubular reactor module are discretized along the flow direction using the standard method of characteristics. According to this method, the tubular reactor is initially discretized into slices that are then followed as smaller batch reactors that are pushed by the process stream, with the same velocity of the local velocity of the flow. The axial position of the slice is tracked continuously during time integration and, as soon as the slice (wave) reaches the reactor outlet, the slice is discarded and a new one is allowed to enter the reactor. The initial condition of the slice is the state of the feed stream of the particular

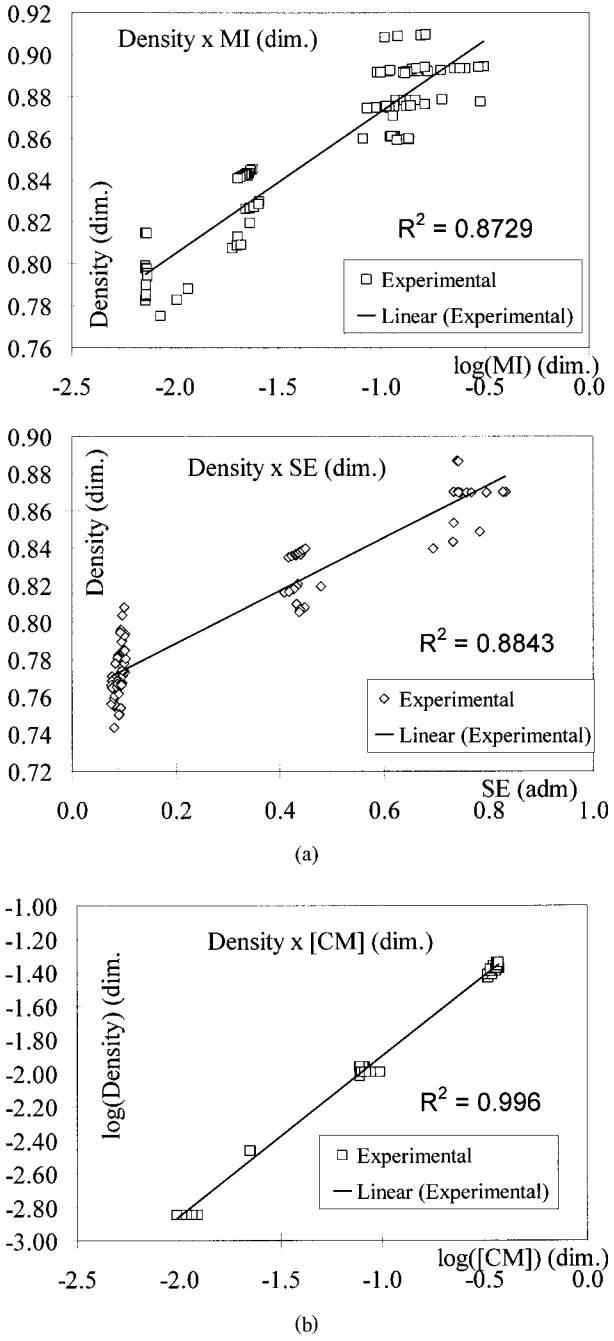

Figure 6 Homopolymer density as a function of *MI* and *SE*.

Table II Parameters Used for Simulation

Property	Parameter	Value	Unit
SE	SE_m	0.0103	Dimensionless
SE	β	−0.048	Dimensionless
SE	SE_M	0.8728	Dimensionless
k_p, k_i	$A_p = A_i$	3.8896×10^2	m^3/(mol s)
k_d, k_t	$A_d = A_t$	13.382	1/s
k_{tH}	A_{tH}	8.7109×10^{-2}	m^3/(mol s)
k_{tE}	A_{tE}	6.6522×10^{-6}	m^3/(mol s)
k_{fH}	A_{fH}	14.503	$(m^3/mol)^{0.5}$/s
k_{fE}	A_{fE}	1.35550×10^{-2}	m^3/(mol s)
k_t	A_t	6.8321×10^4	1/s
k_{fCC}	A_{fCC}	2.6252×10^{-2}	$(m^3/mol)^{0.5}$/s
k_p, k_i	$E_p = E_i$	2.0531×10^4	J/mol
k_d, k_t	$E_d = E_t$	2.5111×10^4	J/mol
k_{tH}	E_{tH}	2.5111×10^4	J/mol
k_{tE}	E_{tE}	2.5111×10^4	J/mol
k_{fH}	E_{fH}	1.455×10^4	J/mol
k_{fE}	E_{fE}	1.455×10^4	J/mol
k_t	E_t	4.645×10^4	J/mol
k_{fCC}	E_{fCC}	1.455×10^4	J/mol
MI	α	4.195×10^{19}	(g/10 min), (g/mol)
MI	β	−3.9252	(g/10 min), (g/mol)
ρ	α	0.9424	g/mL
ρ	β	4.08×10^{-3}	(g/mL), (g/10 min)
ρ	γ	1.094×10^{-2}	g/mL
ρ	δ	−56.37	(g/mL), (% wt)
ρ	ε	0.4668	(g/mL), (% wt)
B	D_0	0.14762	1/s
B	D_f	4.403×10^{-3}	1/(% wt s)
B	D_1	1.061×10^{-3}	1/(A s)

reactor analyzed. As slices reach the reactor outlet discontinuously, a zero-order filter is used to provide flowsheet integration. Therefore, outlet reactor conditions are assumed to be constant between successive waves. Typically, 20 slices were needed to provide accurate numerical results during dynamic integration.

After discretization of the tubular reactor balance equations, a set of algebraic-differential equations is to be solved. The modules regarding the tubular and tank reactors provide both ordinary differential equations and algebraic equations, while the modules regarding the mixers provide only algebraic equations. The integration of the discretized model equations are performed numerically with the code DASSL,[22] which uses backward differentiation formula to discretize and integrate the model. DASSL updates the integration step automatically, depending on the stiffness of the local integration properties of the set of equations.

Model Validation and Simulation

The description of the parameter estimation procedure is beyond the scope of this text and is discussed in detail by Embiruçu et al.[7] for different catalyst systems. It must be stressed, though, that Embiruçu[8] presents all parameters needed for simulation. Table II presents the complete set of parameters needed for simulation of the examples presented below.

Figure 7 shows experimental and simulation results obtained when a grade transition operation is carried out in the plant. During this period, the comonomer feed is replaced by pure ethylene feed. Besides, there is significant hydrogen feed reduction, which causes a significant decrease in the chain transfer reactions. The increase of molecular weight causes significant increase of solution viscosity, decreasing the mixing degree and increasing the temperature gradient. The plant is originally operating with the standard catalyst system at the agitated mode (configuration 1).

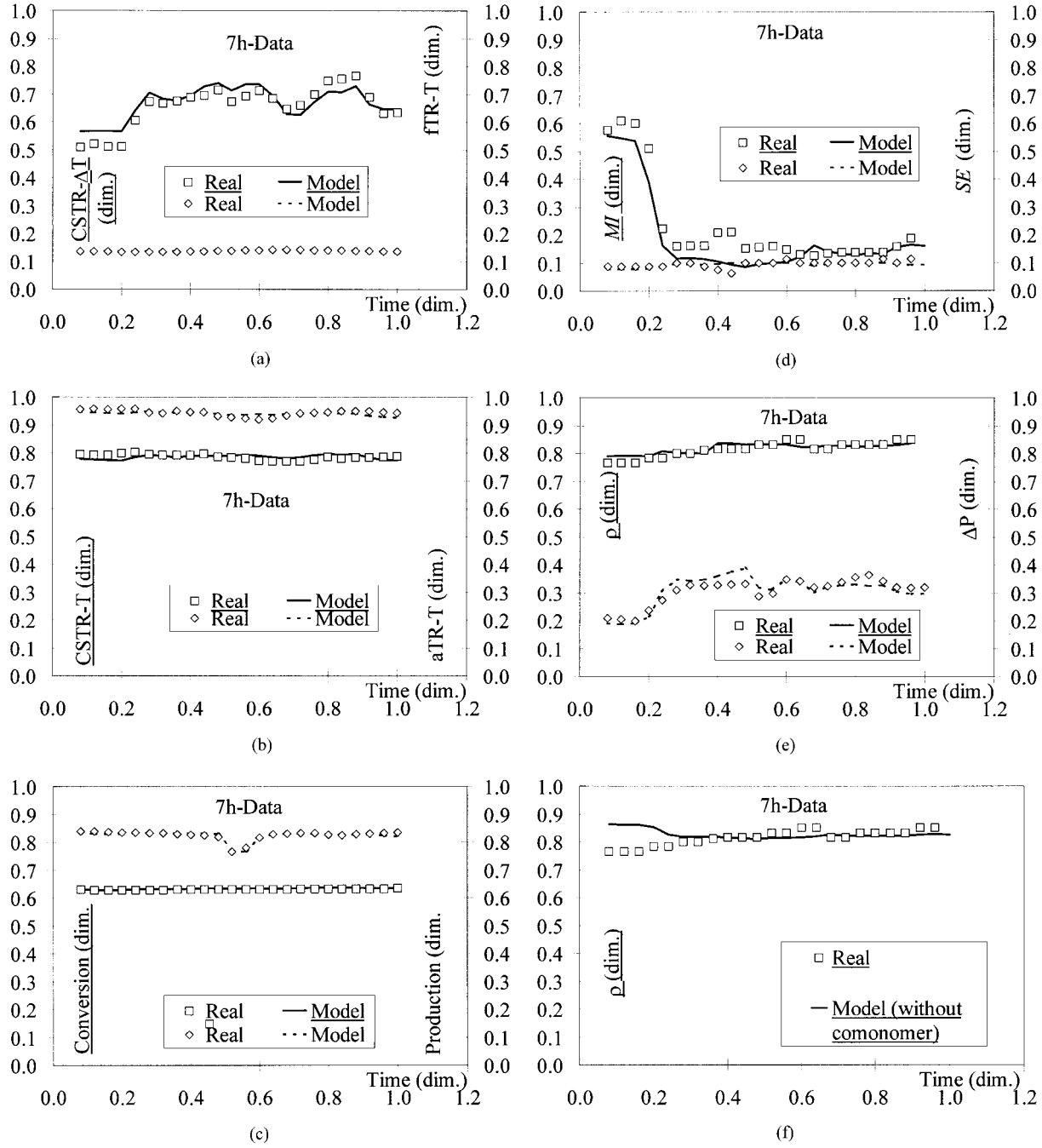

Figure 7 Model and experimental results for the standard catalyst A in the agitated mode. (Units are dimensionless fractions of industrial operation ranges.)

Actual feed conditions and agitator speeds are presented to the model, so that oscillatory responses observed experimentally because of oscillation of the operation conditions can be observed through simulation. Actual process responses are sometimes presented in coded form because of proprietary reasons. Coded variables are presented as a value between 0 and 1, where 0 is the minimum value observed for that variable at plant site and 1 is the maximum value observed for that particular variable at plant site.

Figure 7(a) shows that the model is able to follow the temperature oscillations observed experimentally quite well. The 30% increase of the temperature variation along the CSTR train is intimately connected with the decrease of the ag-

itation efficiency observed after the grade transition. The temperature increase is caused by the increase of the average molecular weight of the polymer resin, which causes additional segregation and increases the nonideality of the mixing conditions. Figure 7(b) shows that the temperature levels along the reactor train are also predicted with good precision, which means that backmixing streams are evaluated adequately. (It must be stressed that plug flow and ideal mixing conditions lead to very different temperature profiles, so that possible deviations of computed temperature profiles are mainly due to improper evaluation of the backmix effect.) The larger the backmixing stream, the smaller the temperature differences along the reactor train. Figure 7(c) shows that, despite the higher temperature differences observed within the reaction train, monomer conversion and polymer productivity change slightly, which confirms that the change of the agitation efficiency is the main cause for increase of reactor temperatures along the train. This also illustrates how important the backmix effect is for this polymerization system.

Figure 7(d) shows the variations observed for the MI and SE. The polymer MI decreases very significantly after the reduction of hydrogen in the feed stream, which indicates the increase of the average molecular weight. As it may be observed, the polymer polydispersity is kept almost constant during the grade transition.

Figure 7(e) shows that both the bulk density and the head loss increase during the grade transition. The increase of the head loss is caused mainly by the decrease of the MI, which causes increase of the solution viscosity. After the removal of comonomer from the feed stream, the bulk density increases because of the reduction of the branching frequency. The model predictions presented for the bulk density in Figure 7(f) is intended to show that the 1-butene content must be inserted into eq. (51) if the model is supposed to be valid for copolymerizations. As observed experimentally, the empirical correction shown in eq. (51) is sufficient to take this effect into consideration. If this is not done, as shown in Figure 7(f), model predictions become biased during copolymerizations.

Figure 8 shows experimental and simulation results obtained when a grade transition is carried out in tubular mode (configuration 2), using the standard catalyst system. In this case, hydrogen is added to the reaction environment at different points of the tubular reactor. Actual feed data are presented for model simulations. In this case, the additional hydrogen feed causes increase of the chain transfer rates and broadening of the MWD, as the concentration of hydrogen changes along the reaction medium. In the case shown in Figure 8, some of the hydrogen feed points are closed during the grade transition, which causes reduction of polydispersity, while the hydrogen feed rates at the initial stages of the reactor are increased, which causes the increase of the MI.

As expected, Figure 8(a–c) show that no significant changes of the temperature levels and polymer productivity are observed, as hydrogen does not affect very much the activity of this particular catalyst system. Steady-state model predictions of temperature and productivity variables are extremely good. The small oscillations observed just after the closing of the control valves perhaps indicate that hydrogen may play a secondary role in catalyst activation and termination for this system. However, as many other operation variables are perturbed simultaneously during grade transitions because of instrument manipulation, this cannot be assured to be true, especially because the final steady-state conditions shown in Figure 8(a–c) are very similar to the original ones.

Figure 8(d) shows that very significant changes of the polymer SE can be observed and that these changes are captured by the model. Although some deviations are present, model predictions are much more reliable in this case, because SE measurements are carried out unfrequently in the laboratory and cannot show fast changes of the polymer properties. Figure 8(d) also shows that the MI is very low and increases during the grade transition, because of the increase of the hydrogen feed rates. Model predictions during grade transition may be regarded as excellent. Figure 8(e) shows that the model is able to predict the small decrease of polymer density and the decrease of the head loss, caused mostly by the increase of the MI. The sensitivity of head losses to variations of the MI is very high, which shows that head losses may be used successfully as an additional variable for the development of inferential models of both polymer productivity and quality for in-line monitoring and control of reactor performance.

The results presented above show that the model is able to describe the dynamic behavior of the solution polymerization of ethylene/1-butene quite well in very complex situations, where different process configurations and feed stream compositions are used. This model can then be

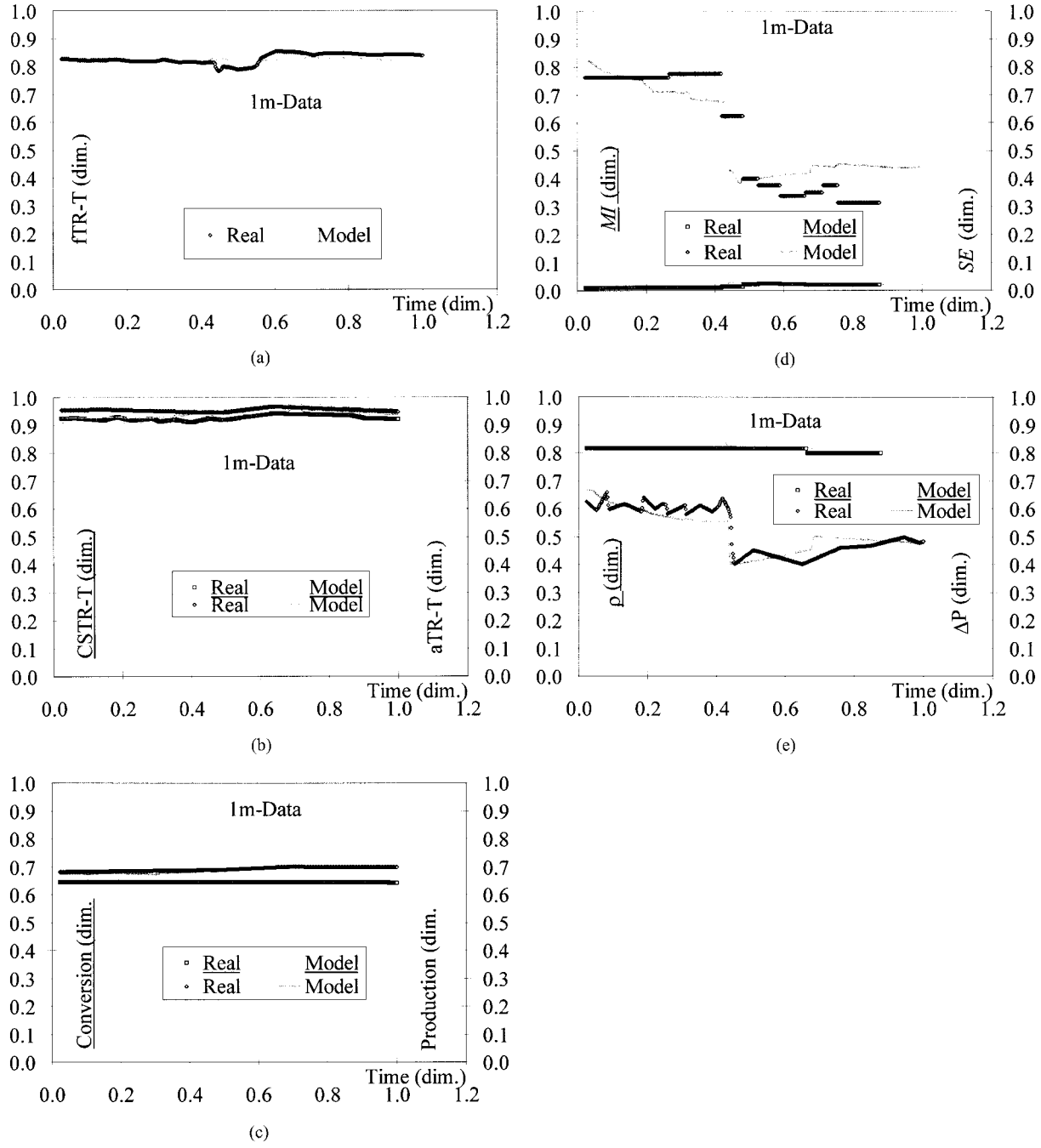

Figure 8 Model and experimental results for the standard catalyst A in the tubular mode. (Units are dimensionless fractions of industrial operation ranges.)

used for simulation of plant performance and for optimization of plant operation, provided that the kinetic parameters for the catalyst system are available. It is important to state that the pseudo-homolymerization approach should not be seen as a model drawback, because it was able to provide a very good description of the dynamics of the copolymerization system. Besides, the model may be easily extended for copolymerization kinetic mechanisms, as discussed previously, and the pseudo-homopolymerization approach allows a very good description of the actual process behavior with a significantly smaller number of parameters obtained directly from the plant, which must be seen as a model advantage.

CONCLUSIONS

A very detailed mechanistic model was developed to represent the solution ethylene polymerization in mixed stirred tank/tubular reactor configurations. The model is based on the detailed kinetic representation of the polymerization, on the individual mass balances for chemical species, and on the energy balances of process equipment. Semiempirical correlations were also developed to model some important end-use polymer properties (such as the MI, the stress exponent, and the bulk polymer density) and process operation variables used routinely to describe the plant operation (such as temperature profiles and head losses in the reaction system). The model was shown to represent very accurately experimental data obtained at plant site during polymer grade transitions, including both ethylene homopolymerizations and ethylene/1-butene copolymerizations. The results obtained show that there is a strong coupling between the polymer properties, the flow characteristics, and the polymerization conditions in these systems, which makes difficult the prediction of final process performance without the help of a process simulator and encourages the use of the model for process simulation and optimization.

NOMENCLATURE

A : Flow transversal area
A_j : Frequency factor for kinetic constant j
B : Backmixing process stream
C : Catalyst
CC : Co-catalysts
CCD : Inactive cocatalyst
CD : Inactive catalyst
Cp : Specific heat capacity
CM : Comonomer
D : Empirical constants for backmixing [eq. (3)]
E_j : Activation energy for kinetic constant j
EA : Active species
f : Weight fraction of lateral feed
F : Lateral feed
G : Term of mass generation
H : Hydrogen
I : Electrical current [eq. (3)]
I_j : Impurities
k_j : Kinetic constant j
K : Empirical constant for pressure drop computations [eq. (40)]
M : Mass
M : Monomer
MI : Melt index
Mw : Weight average molecular weight
Nr : Number of reactor zones
p : Standard weight used for the MI test
P : Live polymer chain
PD : Polydispersion index
PM_j : Molecular weight of species j
r : Reaction rate
R : Side removal stream
R : Universal gas constant, $R = 8.314$ J (mol·K)
S : Solvent
SE : Stress exponent
t : Time
T : Temperature
U : Dead polymer chain
v : Flow velocity
V : Volume
W : Forward feed flow rate
WQ : Volumetric flowrate
x : Conversion
z : Axial position

Greek

$\alpha, \beta, \delta, \gamma$: Empirical constants
ΔH : Heat of reaction
ΔP : Head loss
λ_j : j^{th} moment of the size distribution of dead polymer chains
μ_j : j^{th} moment of the size distribution of live polymer chains
μ : Viscosity
ρ : Density

Subscripts

0 : Initial condition
d : Deactivation
e : Inlet stream
f : Espontaneous transfer
fCC : Transfer to cocatalyst
fH : Transfer to hydrogen
i : Initiation
IC : Catalyst poison
ICC : Cocatalyst poison
n : Active species n
p : Propagation
r : Reactor zone
s : outlet stream
t : Espontaneous termination
tE : Termination by ethylene
tH : Termination by hydrogen

u : Dead polymer

Superscripts

$\cdot$: Active species

Others

[ ] : Molar concentration

REFERENCES

1. Eliçabe, G. E.; Meira, G. R. Polym Eng Sci 1988, 28, 121.
2. MacGregor, J. F.; Penlidis, A.; Hamielec, A. E. Polym Proc Eng 1984);2, 179.
3. Kelly, S. J.; MacGregor, J. F.; Hoffman, T. W. Can J Chem Eng 1987);65, 852.
4. Choi, K. Y. J Appl Polym Sci 1985);30, 2707.
5. Cozewith, C. AIChE J 1988);34, 272.
6. Kim, K. J.; Choi, K. Y. AIChE J 1991);37, 1255.
7. Embiruçu, M.; Lima, E. L.; Pinto, J. C. J Appl Polym Sci, submitted.
8. Keii, T. Kinetics of Ziegler-Natta Polymerization; Tokyo, Japan: Kodansha Ltd., 1972.
9. Dutschke, J.; Kaminsky, W.; Lüker, H. In: Polymer Reaction Engineering; Reichert, K. H.; Geiseler, W., eds. Müchen, Germany, Hanser, 1983, p 207.
10. Fink, G.; Fenzl, W.; Mynott, R. In: Keii, T.; Soga, K., eds.; Proceedings of the International Symposium on Future Aspects of Olefin Polymerization; Tokyo, Japan: Kodansha/Elsevier, 1986, p 215.
11. Costa, M. A. S. DSc. Thesis, IMA/Universidade Federal do Rio de Janeiro, Rio de Janeiro, Brazil, 1995.
12. van der Ven, S. Polypropylene and Other Polyolefins—Polymerization and Characterization, Studies in Polymer Science 7; Amsterdam: Elsevier, 1990.
13. Marques, M. M. V.; Nunes, C. P.; Tait, P. J. T.; Dias, A. R. J Polym Sci Polym Chem 1993, 31, 209.
14. Marques, M. M. V.; Nunes, C. P.; Tait, P. J. T.; Dias, A. R. J Polym Sci Polym Chem 1993, 31, 219.
15. Ray, W. H. J Macromol Sci Rev Macromol Chem 1972, C8, 1.
16. Nielsen, L. E. Polymer Rheology; New York: Marcel Decker, 1977.
17. Carrot, C.; Revenu, P.; Guillet, J. J Appl Polym Sci 1996, 61, 1887.
18. Gahleitner, M.; Bernreitner, K.; Neißl, W., Paulik, C.; Ratajski, E. Polym Test 1995, 14, 173.
19. Gahleitner, M.; Wolfschwenger, J.; Bachner, C.; Bernreitner, K.; Neißl, W. J Appl Polym Sci 1996, 61, 649.
20. Schultz, B. Operation Data for Grade Transitions; Politeno S. A., 1996.
21. Embiruçu, M. DSc. Thesis, PEQ / COPPE / Universidade Federal do Rio de Janeiro, Rio de Janeiro, Brazil, 1998.
22. Petzold, L. R. DASSL: A Differential-Algebraic System Solver; Livermore, CA: Computer and Mathematical Research Division, Lawrence Livermore National Laboratory, 1989.